Chemical Physics Letters 691 (2018) 238–242

Contents lists available at ScienceDirect

Chemical Physics Letters

journal homepage: www.elsevier.com/locate/cplett

Research paper

Activated carbon derived from harmful aquatic plant for high stable supercapacitors

Jiangfeng Li [a,*], Qingsheng Wu [b]

[a] Department of Chemistry, Lishui University, Lishui 323000, PR China
[b] School of Chemical Science and Engineering, Tongji University, Shanghai 200092, PR China

ARTICLE INFO

Article history:
Received 4 August 2017
In final form 15 November 2017
Available online 15 November 2017

Keywords:
Harmful aquatic plant
Carbon materials
Porous materials
High stability
Supercapacitor

ABSTRACT

Considering cost and environmental protection, the harmful aquatic plant altemanthera philoxeroides derived carbon material with super high specific surface area (2895 $m^2 g^{-1}$) is an ideal electrode material for supercapacitor. The structure and composition of these carbon materials were characterized by SEM, EDS, XPS and BET measurements. The obtained material exhibits a maximum specific capacitance of 275 $F g^{-1}$ at 0.5 $A g^{-1}$ and retains a capacitance of 210 $F g^{-1}$ even at 50 $A g^{-1}$. In addition, it also shows excellent capacity retention of 5000 cycles at 10 $A g^{-1}$.

1. Introduction

Supercapacitors as an ideal energy-storage device have attracted plenty attentions due to their high power density, long cycle life, and fast charging time [1–3]. According to the charge-storage mechanism, it can be separated into two categories: double layer capacitors (EDLCs) and pseudocapacitors. The energy storage of EDLCs has been derived from the nonfaradic surface charge accumulation at electrode and electrolyte interfaces. Recently, biomass derived activated carbon as electrode for supercapacitors have been attracted extensive attention due to their unique structure, high specific surface area, low-cost and abundant porosity than other carbon materials [4].

Altemanthera philoxeroides (AP), an extremely common kind of harmful aquatic plant, is a native of South America and naturalized in China since the 1930s. Until now, it has been around the world due to its extremely reproductive ability and hard to manipulate. In this study, we, for the first time, demonstrate the synthesis of activated carbon by the activation of AP for supercapacitors.

2. Experimental

The AP was cleaned with deionized water, dried in an oven, pre-carbonized at 450 °C. The pre-carbonized carbon was ground to powder, immersed into KOH aqueous solution, and activated at 800 °C. The final products were mixed with excess 3 M HCl solution, washed with deionized water and finally dried in an oven at 80 °C. The final materials are denoted as APPC-n, where n is the weight ratio of KOH to pre-carbonized materials.

The morphology and elemental compositions of the samples were characterized by field emission scanning electron microscope (SEM, Hitachi S-4800), X-ray photoelectron spectroscopy (XPS, AXIS Ultra DLD), energy dispersive spectroscope (EDS) and transmission electron microscopy (TEM, JEOL JEM-2100). Powder X-ray diffraction (XRD) patterns were analyzed from Bruker Focus D 8 diffract-meter with Cu Kα radiation (40 kV, $\lambda = 0.15418$ nm) between 10 and 80°. The porous natures were characterized by N_2 adsorption at 77 K using ASAP 3020 Micromeritics volumetric system. The specific surface area was tested by the Brunauer-Emmette-Teller (BET) method. The electrode was synthesized by mixing the materials, acetylene black and PTFE in a weight ratio of 85:10:5. The electrochemical characterizations were tested in 6 M KOH electrolyte on a CHI 660D electrochemical workstation.

3. Results and discussion

3.1. Structural and morphological characteristics

As shown in Figs. 1 and S1, all the materials have a poriferous and lax structure with a large number of obvious holes on the rough surface. As shown in Fig. 1(C), the porous structure of APPC-4 has been slightly damaged due to the excessive addition of KOH [5]. As shown in Fig. 1(D), the porous structure of APPC-3

* Corresponding author.
E-mail address: lijiangfeng@lsu.edu.cn (J. Li).

https://doi.org/10.1016/j.cplett.2017.11.031
0009-2614/

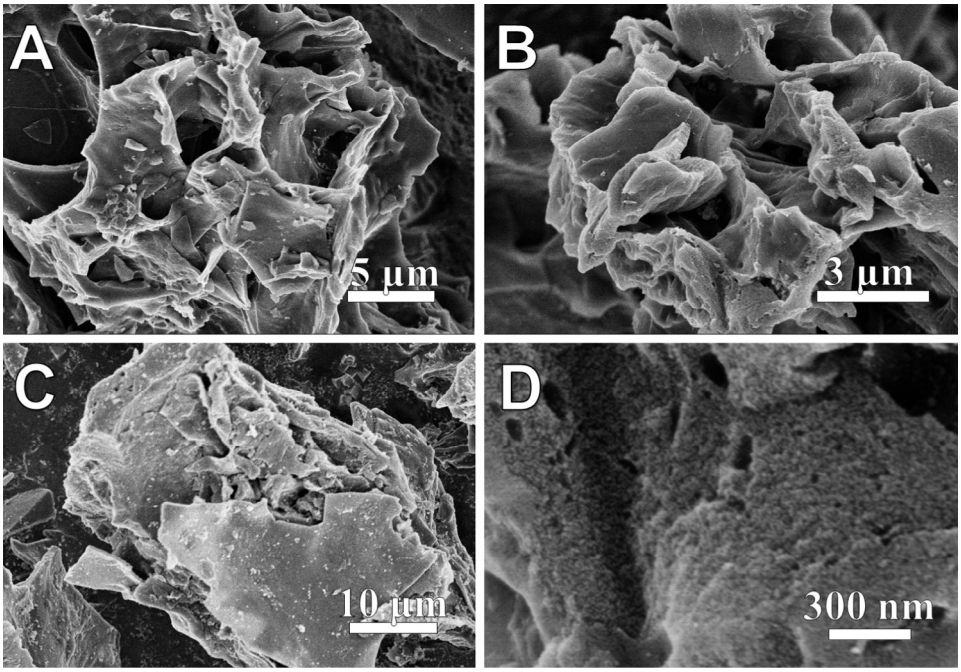

Fig. 1. SEM images of APPC-2 (A), APPC-3 (B, D) and APPC-4 (C).

has been clearly observed and the average pore size is in the range of 2–20 nm. The TEM image in Fig. 2(A) presents that the pore size of APPC-3 is less than ~1.5 nm, which could be due to the KOH activation and contribute to the absorption of electrolyte ions.

Figs. 2(B) and S2A show the N_2 sorption isotherms and pore size distribution profiles of APPCs. All the N_2 isotherms show a typical type-I isotherm with H_4 type hysteresis loop, which indicates the microporous character of these samples [6]. The pore size distribution profiles of APPCs are shown in the inset of Fig. 1(B) and S2A. These APPCs have a similar pore size distribution ranges from 0.7 to 5 nm, indicating the coexistence of micropore and mesopore structures. During in the electrochemical reaction, mesopores

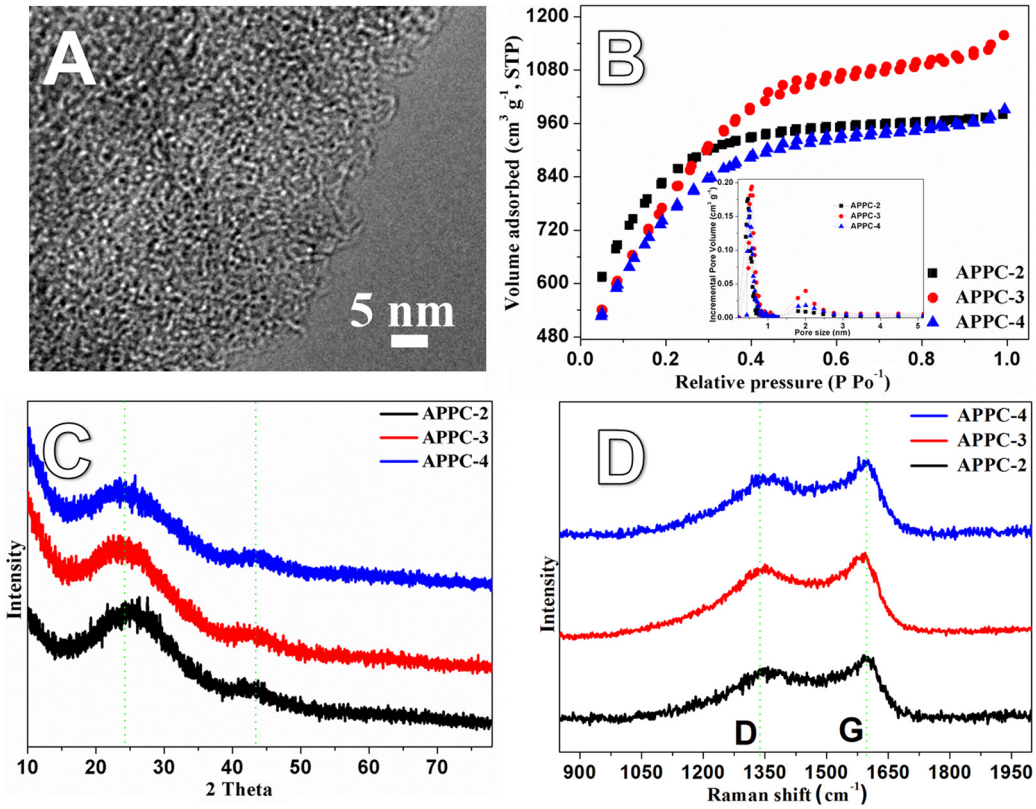

Fig. 2. (A) TEM image of APPC-3; (B) nitrogen sorption isotherms, (C) XRD pattern (Inset: pore size distribution profiles of APPCs) and (D) Raman spectra of APPCs.

(2–50 nm) can provide effective path for the fast transport of electrolyte ions and then could generate a good rate capacity, while the solvated/desolvated counterions could line up along the inner pore axis and form an electric wire-in-cylinder capacitor in the micropore regime (<2 nm) [7]. As depicted in Table S1, the measured pore volumes are 1.57, 1.99 and 1.51 $cm^3\ g^{-1}$ with the pore size is 2.54, 2.26 and 2.39 nm for APPC-2, APPC-3 and APPC-4, respectively. Obviously, APPC-3 has a higher pore volume and lower pore size, which indicates the appropriate weight of KOH can lead to the higher pore volume and proper pore size distribution. As shown in Fig. 2(C), there are two obvious peaks located at around 24.9° (0 0 2) and 44.5° (1 0 0). It indicates that all samples have a well degree of graphitization, which could enhance the materials' electrical conductivity [8]. In addition, there are two typical peaks located at around 1346 cm^{-1} (D band) and 1586 cm^{-1} (G band) in Figs. 2(D) and S2B, indicates all these samples have a high degree of graphitization [9]. In addition, the higher G/D ratio of band intensities indicates the higher degree of graphitization and electrical conductivity of the samples [4]. Here, the G/D intensity ratio of APPC-0, APPC-2, APPC-3 and APPC-4 were determined to be 1.18, 1.13, 1.08 and 0.94, respectively. The G/D intensity ratio is reduced with the increased weight ratio of KOH to char. It reveals more defects were introduced in APPC-4 due to the activation of carbon atoms with KOH, which leaves rich oxygen-containing functional groups as indicated by a high oxygen content of APPC-4.

As shown in Table S2, the contents of O are gradually increased while the contents of C are gradually decreased with increasing the weight ratio of KOH/char. It indicates that the KOH activation process could improve the contents of oxygenic groups of the carbon materials. Fig. S3 shows the high-resolution C1s and O1s XPS spectra. In the C1s spectra, a narrow trend is clearly observed indicates a high degree of graphitic order [10]. The binding energy centered at around 284.8 eV in the C1s spectra belongs to —C— or —C—H, which could enhance the materials' conductivity [11]. Meanwhile, the other two peaks centered at around 285.7 eV and 288.7 eV are assigned to —C═O and O═C—O— respectively, which could induce faradaic reactions [12]. In the O1s spectra, two peaks located at around 533.4 eV (═O) and 537.1 eV (O═C—OH) could induce faradaic reactions and improve the wettabilitys [13]. The surface of O═C—OH is increased with the increased weight ratio of KOH to char, which could be due to the KOH activation.

3.2. Electrochemical properties

The electrochemical performance was measured in a three electrode system. Fig. 3(A)–(C) and Fig. S4A show the cyclic voltammetry (CV) curves of these APPCs. A symmetric shape is clearly observed in all CV curves, indicates a typical double-layer capacitive behavior [13]. Compared with APPC-0, the other three samples keep a more rectangular-like shape, which dues to the higher specific surface and pore volume.

In order to value the electrochemical property of those samples, the galvanostatic charge/discharge (GCD) technique has been used and the results depicted in Figs. 3(D)–(F) and S4B. All GCD curves show an approximately triangular-like shape indicating a low

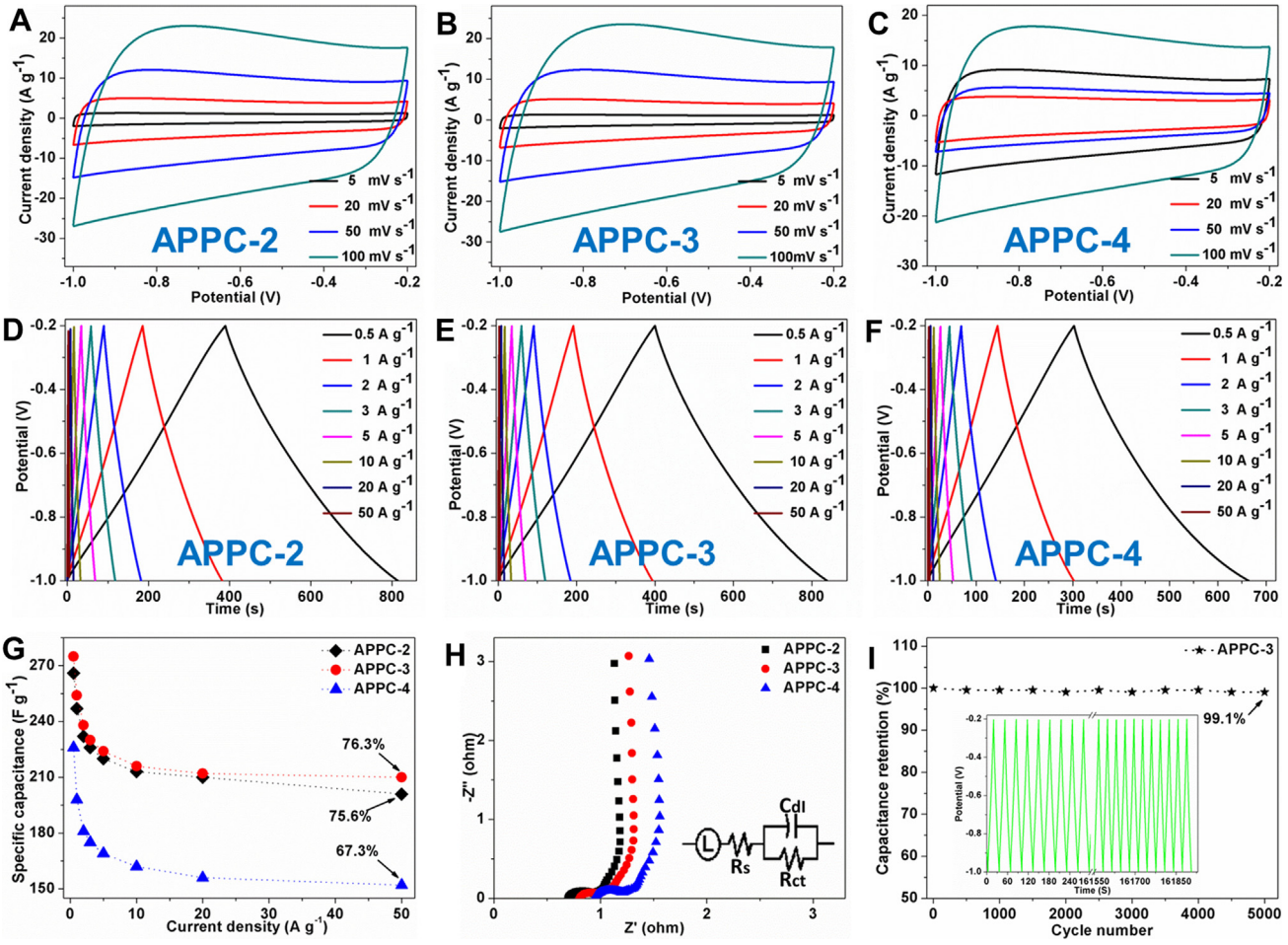

Fig. 3. The CV curves of APPC-2 (A), APPC-3 (B) and APPC-4 (C). The GCD curves of APPC-2 (D), APPC-3 (E) and APPC-4 (F). The specific capacitance values (G) and Nyquist impedance curves (H) of APPCs. Cycle stability of APPC-3 (I) at 10 A g^{-1} for 5000 cycles (inset: GCD curves).

resistance and good conductivity. However, a little curvature has been observed in all GCD curves at 0.5 A g^{-1} due to the trace amounts of oxygenic groups [14]. The specific capacitance values of all APPCs are present in Figs. 3(G) and S4C. The APPC-3 based electrode exhibits a maximum specific capacitance of 275 F g^{-1} at 0.5 A g^{-1}. It might be due to the higher pore volume, proper pore size distribution and a small amount of oxygenic groups. Even at 50 A g^{-1}, APPC-3 still keeps specific capacitance of 210 F g^{-1} (76.3% capacitance retention from 0.5 A g^{-1} to 50 A g^{-1}).

The Nyquist plots of these electrodes are present in the Figs. 3 (H) and S4D. The semicircle in the high frequency region reflects the charge transfer resistance (*R*ct), while the intercept of the plots with the X-axis reflects the solution resistance of the electrochemical system (*Rs*). The Nyquist plot can be fitted with an equivalent circuit for impedance analysis (inset in Fig. 3(H)), where *Rs* is the solution resistance of the electrochemical system, *Rct* is Faradaic interfacial charge transfer resistance and C_{dl} is double layer capacitor. As shown in Fig. 3(H), APPC-2, APPC-3 and APPC-4 have the Rs of 0.70, 0.81 and 0.94 Ω with the Rct of 0.25, 0.16 and 0.27 Ω, respectively. The increased Rs might be due to the improved oxygenic groups, which could reduce the ability of electrolyte ion adsorption and diffusion. The lower *R*ct of APPC-3 dues to its higher pore volume, which could promote the ion access to the inner fast.

Fig. 3(I) shows the retention of specific capacitance with the increasing cycle number. The specific capacitance has a little damage over 5000 cycles and it retains 99.1% of the initial specific capacitance. The little dropping in the specific capacitance could be due to the irreversible reaction between the electrode and electrolyte. In addition, the inset in Fig. 4(I) shows the GCD curve still maintains a symmetrical shape over 5000 cycles, which is due to the high specific surface area and abundant porosity.

Table 1 compared the specific capacitance, specific capacitance retention and cyclic stability of various reported carbon materials synthesized from nature plants. The activated carbon derived from AP exhibits a perfect electrochemical performance in comparison

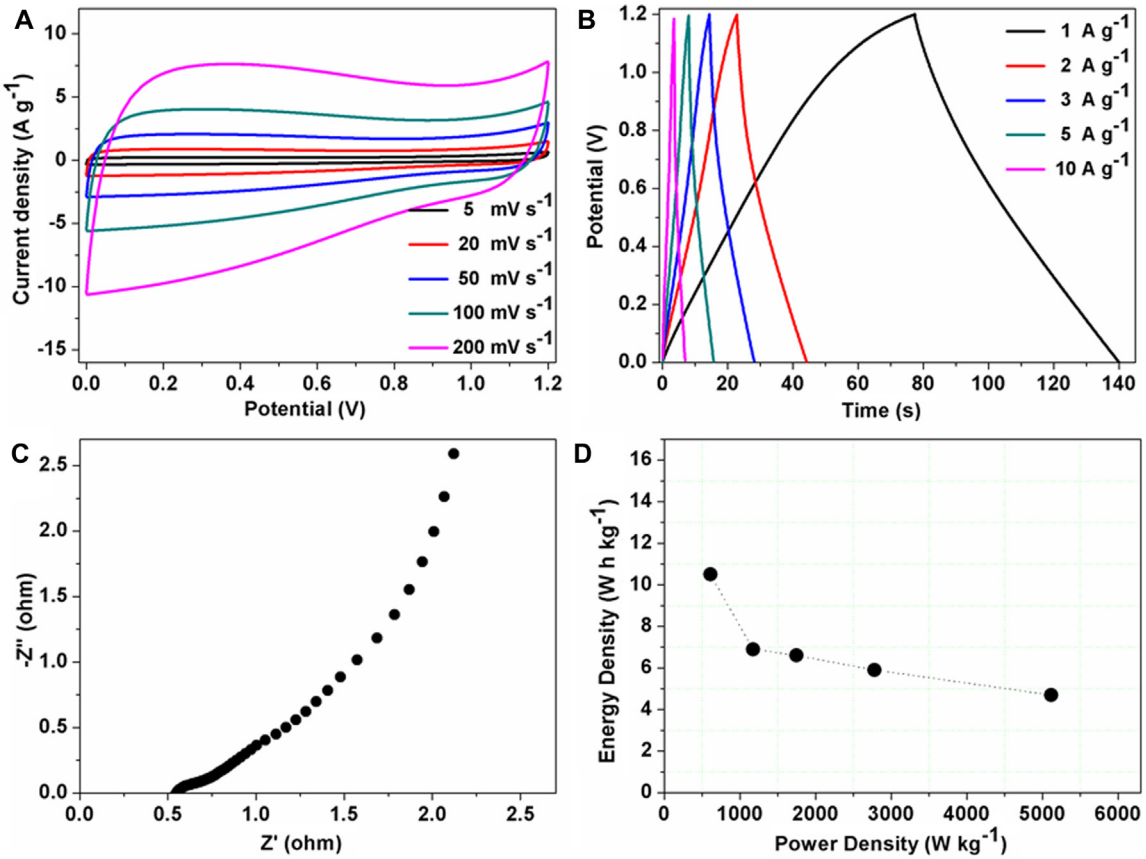

Fig. 4. The electrochemical performance of as-assembled symmetric supercapacitor (APPC-3//APPC-3) was measured in 6M KOH electrolyte at room temperature: (A) CV curves at different scan rates, (B) GCD curves at various current densities, (C) Nyquist plots in the frequency range from 10^{-1} Hz to 10^{6} Hz, and (D) Ragone plot of the symmetrical system.

Table 1
Comparison of electrochemical performance of porous carbon derived from plant precursors in a three-electrode system.

Materials	Electrolyte	Maximum capacitance (F g^{-1})	Rate capability (%)	Cycling stability (%)
AP	6M KOH	275 (0.5 A g^{-1})	76.3 (up to 50 A g^{-1})	99 (5000 cycles)
Broad beans [15]	1M H_2SO_4	202 (0.5 A g^{-1})	64 (up to 10 A g^{-1})	90 (3000 cycles)
Water hyacinth [16]	6M KOH	273 (1 A g^{-1})	77 (up to 50 A g^{-1})	99 (5000 cycles)
Biochar [17]	6M KOH	260 (0.6 A g^{-1})	88 (up to 1 A g^{-1})	99 (2000 cycles)
Lignin [18]	1M H_2SO_4	165 (0.05 A g^{-1})	74 (up to 10 A g^{-1})	97 (5000 cycles)
Brussel sprouts [19]	6M KOH	255 (0.5 A g^{-1})	83 (up to 50 A g^{-1})	99 (5000 cycles)
Water bamboo [20]	6M KOH	268 (0.5 A g^{-1})	83 (up to 10 A g^{-1})	97 (5000 cycles)
Bagasse [21]	6M KOH	268 (2 mV s^{-1})	75 (up to 200 mV s^{-1})	\
Shiitake [22]	6M KOH	300 (1 A g^{-1})	77 (up to 30 A g^{-1})	\

to water bamboo, barks, water hyacinth, etc. The superior electrochemical performance of APPC-3 could be due to the high pore volume, proper pore size, and oxygenic groups.

To investigate the electrochemical properties of altemanthera philoxeroides derived carbon material for practical application, a symmetric two electrode cell (APPC-3//APPC-3) was assembled by using APPC-3 both as positive and negative electrodes in 6 M KOH electrolyte in the potential range of 0 to 1.2 V. As shown in Fig. 4(A), the CV curves of APPC-3//APPC-3 at low scan rate (5 mV s^{-1}) maintain a symmetric and rectangular shape, which indicates a typical double-layer capacitive behavior. In addition, the CV curves show a little departure from the rectangular shape at high scan rates, which is due to large ohmic resistance and slow charge propagation. Fig. 4(C) shows the Nyquist plot of APPC-3//APPC-3 in the frequency range from 10^{-1} Hz to 10^{6} Hz. As shown in Fig. 4(C), the Nyquist plot can be separated into two parts: a semicircle at the mid frequency region and accompanied with a straight line at low region, which indicates a typical double layer capacitor behavior. In addition, the as-assembled symmetric supercapacitor has low series equivalent resistances (Rs + Rct), which indicates the electrode material and current collector are attached well. Fig. 4(B) shows the GCD curves of the symmetric supercapacitor at various current densities. All the GCD curves keep a symmetric triangle shape with a little IR drop, indicates good capacitive characteristics. Fig. 4(D) shows the Ragone plot of the as-assembled symmetric supercapacitor. The energy density can reach up 10.5 W h kg^{-1} at a power density of 608 W kg^{-1} and 5.9 W h kg^{-1} at a power density of 2777 W kg^{-1}, which is superior to the commercial devices (<3 W h kg^{-1}) [23]. In conclusion, the altemanthera philoxeroides derived carbon materials with a small amount of oxygen-containing groups might be an ideal electrode material for supercapacitor and has a broad potential commercial application prospect as the carbon precursor is very cheap and synthesis method is very easy.

4. Conclusion

In summary, this study provides a simple and efficient conversion of a harmful aquatic plant to a valuable material. The activated carbon exhibit a maximum specific capacitance of 275 F g^{-1} at 0.5 A g^{-1}, high rate capability and excellent cycling stability. This high supercapacitor performance can be attributed to the high specific surface area (2895^2 g^{-1}), abundant porosity and a small amount of oxygenic groups.

Appendix A. Supplementary material

Supplementary data associated with this article can be found, in the online version, at https://doi.org/10.1016/j.cplett.2017.11.031.

References

[1] W. Tian, Q. Gao, Y. Tan, et al., Bio-inspired beehive-like hierarchical nanoporous carbon derived from bamboo-based industrial by-product as a high performance supercapacitor electrode material, J. Mater. Chem. A 3 (2015) 5656–5664.
[2] H. Jiang, P.S. Lee, C. Li, 3D carbon based nanostructures for advanced supercapacitors, Energ. Environ. Sci. 6 (2012) 41–53.
[3] G.X. Zhu, C. Xi, Y. Liu, J. Zhu, X.P. Shen, CN foam loaded with few-layer graphene nanosheets for high-performance supercapacitor electrode, J. Mater. Chem. A 3 (2015) 7591–7599.
[4] W. Qian, F. Sun, Y. Xu, et al., Human hair-derived carbon flakes for electrochemical supercapacitors, Energ. Environ. Sci. 7 (2014) 379–386.
[5] D. Bhattacharjya, J.S. Yu, Activated carbon made from cow dung as electrode material for electrochemical double layer capacitor, J. Power Sources 262 (2014) 224–231.
[6] Y.S. Su, A. Manthiram, Lithium-sulphur batteries with a microporous carbon paper as a bifunctional interlayer, Nat. Commun. 3 (2012) 1166.
[7] J. Huang, B.G. Sumpter, V. Meunier, A universal model for nanoporous carbon supercapacitors applicable to diverse pore regimes, carbon materials, and electrolytes, Chemistry 14 (2008) 6614.
[8] J.P. Paraknowitsch, J. Zhang, D. Su, A. Thomas, M. Antonietti, Ionic liquids as precursors for nitrogen-doped graphitic carbon, Adv. Mater. 22 (2010) 87.
[9] D.W. Wang, F. Li, J. Zhao, et al., Fabrication of Graphene/polyaniline composite paper via in situ anodic electropolymerization for high-performance flexible electrode, ACS Nano 3 (2009) 1745–1752.
[10] H. Zhu, X. Wang, X. Liu, X. Yang, Integrated synthesis of poly(o-phenylenediamine)-derived carbon materials for high performance supercapacitors, Adv. Mater. 24 (2012) 6524–6529.
[11] J.P. Paraknowitsch, B. Wienert, Y. Zhang, A. Thomas, Intrinsically sulfur- and nitrogen-co-doped carbons from thiazolium salts, Chem. A Eur. J. 18 (2012) 15416–15423.
[12] J. Ding, H. Wang, Z. Li, et al., Peanut shell hybrid sodium ion capacitor with extreme energy–power rivals lithium ion capacitors, Energ. Environ. Sci. 8 (2015) 941–955.
[13] S. Wang, Z. Ren, J. Li, et al., Cotton-based hollow carbon fibers with high specific surface area prepared by ammonia etching for supercapacitor application, RSC Adv. 4 (2014) 31300–31307.
[14] V. Barranco, M.A. Lillo-Rodenas, A. Linares-Solano, et al., Amorphous carbon nanofibers and their activated carbon nanofibers as supercapacitor electrodes, J. Phys. Chem. C 114 (2010) 10302–10307.
[15] G.Y. Xu, J.P. Han, D. Bing, et al., Biomass-derived porous carbon materials with sulfur and nitrogen dual-doping for energy storage, Green Chem. 17 (2015) 1668–1674.
[16] K. Wu, B. Gao, J. Su, et al., Large and porous carbon sheets derived from water hyacinth for high-performance supercapacitors, RSC Adv. 6 (2016) 29996–30003.
[17] H. Jin, X. Wang, Z. Gu, J. Polin, Carbon materials from high ash biochar for supercapacitor and improvement of capacitance with HNO_3 surface oxidation, J. Power Sources 236 (2013) 285–292.
[18] W. Zhang, P.H. Lin, Z. Lin, et al., 3D hierarchical porous carbon for supercapacitors prepared from lignin through a facile template-free method, ChemSusChem 8 (2015) 2114–2122.
[19] J. Li, G. Zan, Q. Wu, Nitrogen and sulfur self-doped porous carbon from brussel sprouts as electrode materials for high stable supercapacitors, RSC Adv. 6 (2016).
[20] J. Li, Q. Wu, Water bamboo-derived porous carbons as electrode materials for supercapacitors, New J. Chem. 39 (2015) 3859–3864.
[21] P. Hao, Z. Zhao, J. Tian, et al., Hierarchical porous carbon aerogel derived from bagasse for high performance supercapacitor electrode, Nanoscale 6 (2014) 12120–12129.
[22] P. Cheng, S. Gao, P. Zang, et al., Hierarchically porous carbon by activation of shiitake mushroom for capacitive energy storage, Carbon 93 (2015) 315–324.
[23] Y. Gogotsi, P. Simon, Science 334 (2011) 917–918.